CHAPTER 3

MICROSTRUCTURAL CHARACTERIZATION

This chapter presents a detailed investigation into the influence of austempering time on the microstructure, phases, crystallite size, lattice microstrain, dislocation density, and carbon concentration in the retained austenite of austempered steel. Additionally, it discusses the comprehensive microstructural characterization of patented steel, providing valuable insights into the effects of the patenting process on the steel's properties. The changes in the microstructure were investigated using a combination of optical microscopy, scanning electron microscopy (SEM), transmission electron microscopy (TEM) techniques and electron back scattered diffraction (EBSD) analysis. These advanced imaging techniques allowed for a comprehensive analysis and characterization of the microstructural modifications. X-ray diffraction is used to identify the phases, estimation of volume fraction of phases, crystallite size, lattice microstrain, dislocation density and carbon content in austenite.

3.1 OPTICAL MICROSTRUCTURE

Optical microscopy of samples B12VA-1, B12VA-2, B14VA-1, B14VA-2, B15VA-1, and B15VA-2 demonstrates a two-phase microstructure with the plate-like morphology of bainite (dark region) and blocky retained austenite (white region) (Figure 3.1 a-f). Significantly less blocky austenite (Υ_B) is seen in B12VA-2, B14VA-2, and B15VA-2 than that in B12VA-1, B14VA-1, and B12VA-1, respectively, although the quantity of bainite is increased. The optical microscopy analysis revealed that the patented steel samples, namely P12VA, P14VA, and P15VA, exhibit a distinctive pearlitic morphology, as depicted in Figure 3.2a-c.

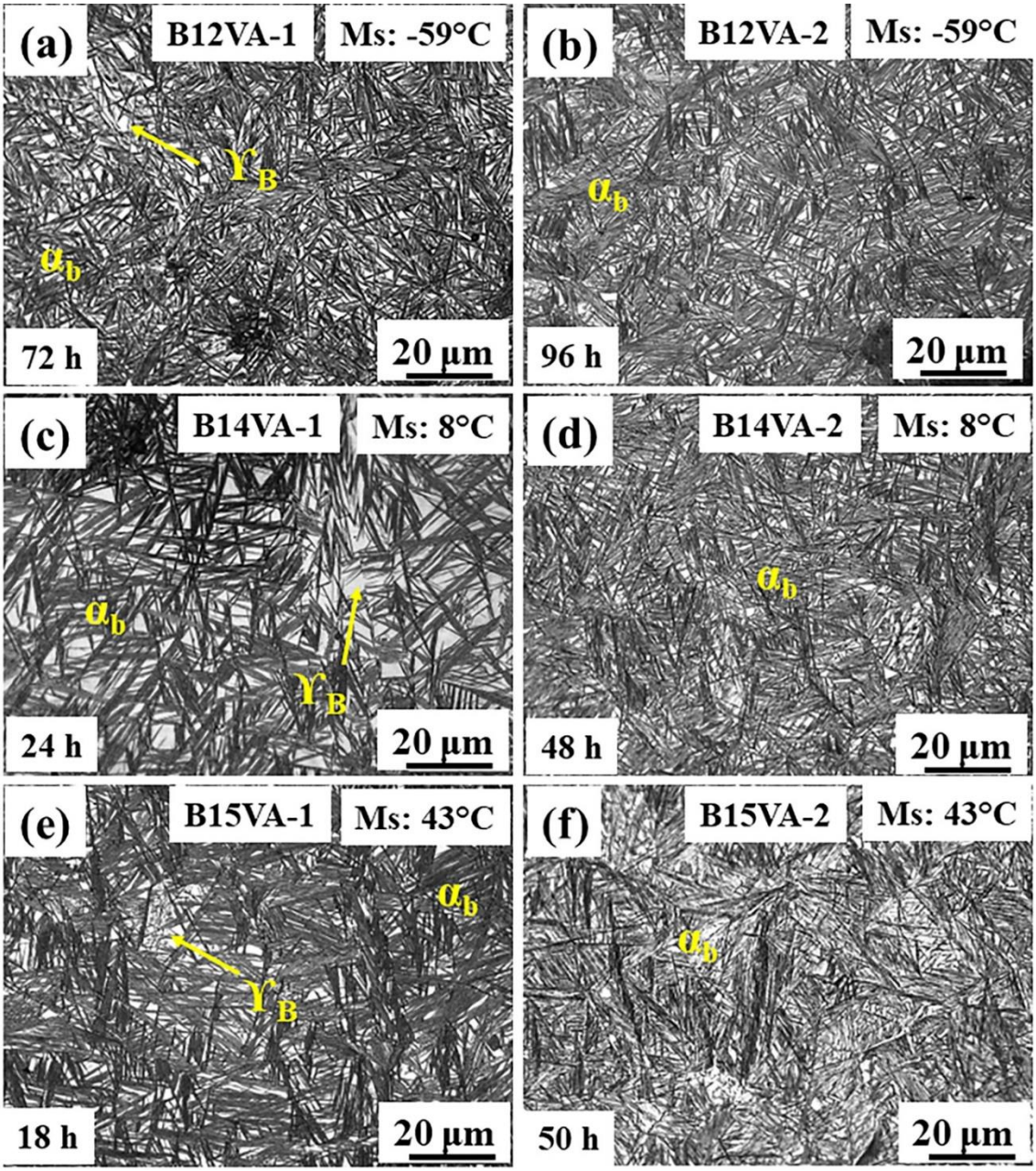

Figure 3.1 Optical microstructure of the austempered (at 250°C) steels (a) B12VA-1, (b) B12VA-2, (c) B14VA-1, (d) B14VA-2, (e) B14VA-1, and (f) B15VA-2.

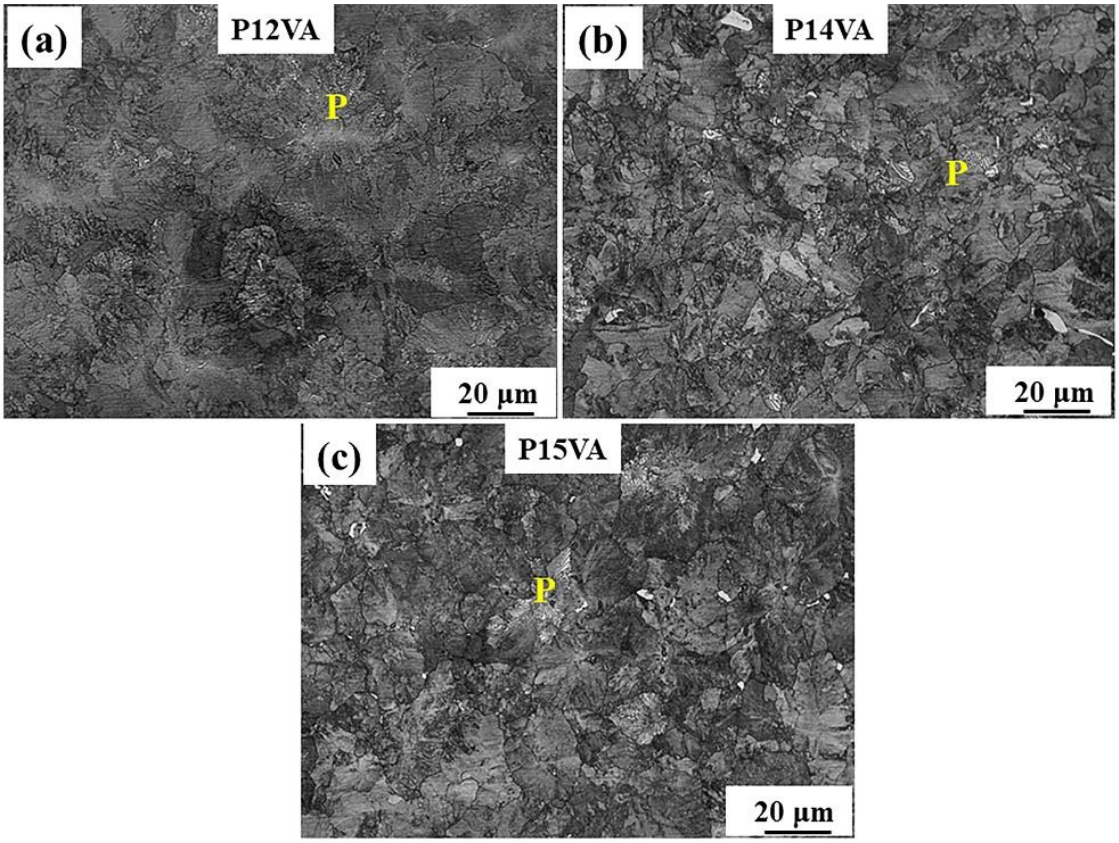

Figure 3.2 Optical microstructure of the pearlitic steels at 550°C: (a) P12VA, (b) P14VA and (c) P15VA.

3.2 X-RAY DIFFRACTION

Figure 3.3 shows the XRD patterns of B12VA, B14VA and B15VA steels, austempered for the different duration. In Figure 3a, the XRD patterns of B12VA-1 clearly depict the peak intensities corresponding to bainite and retained austenite phases, while no peak intensity associated with carbide (cementite) is observed. The calculated crystallite sizes (using Equation 2.4) for the retained austenite and bainite are determined to be 46.2 nm and 42.1 nm, respectively (as shown in Table 3.1). The lattice strain of the retained austenite and bainite is estimated (using Equation 2.5) to be 0.28% and 0.30%, respectively (also shown in Table 3.1). The dislocation density in the retained austenite and bainite is evaluated (using Equation 2.6) to be $9.78 \times 10^{16}/m^2$ and $8.28 \times 10^{16}/m^2$, respectively. For the B12VA-1 sample, the volume fraction of retained austenite and

bainite is estimated (using Equation 2.2) to be 48% and 52%, respectively, with a calculated volume fraction of 7.8% for filmy austenite (using Equation 2.3) and 40.2% for blocky austenite (as presented in Table 3.1). Additionally, the retained austenite phase is found to have a carbon concentration of 1.49 mass% (using Equation 2.7) (as indicated in Table 3.1).

Figure 3.3b depicts the XRD pattern of B12VA-2. The patterns of B12VA-2 also show the bainite and retained austenite peaks but lower peak intensities of retained austenite than that of B12VA-1 and no carbide peak. The estimated crystallite sizes of retained austenite and bainite are 35.7 nm and 36.4 nm, respectively. The lattice strains of retained austenite and bainite are 0.35% and 0.33%, respectively. The dislocation density in retained austenite and bainite are 12.66 $x10^{16}/m^2$ and 13.10 $x10^{16}$ $/m^2$, respectively (Table 3.1). The calculated volume fraction of retained austenite and bainite for the B12VA-2 sample are 35% and 65%, respectively and the estimated volume fraction of filmy austenite and blocky austenite are 9.8% and 25.3%, respectively (Table 3.1). Carbon concentration in retained austenite is calculated to be 1.60 mass % (Table 3.1).

In Figure 3c, the XRD patterns of B14VA-1 exhibit distinct peak intensities corresponding to the bainite and retained austenite phases, with no observable peak intensity related to carbide (cementite). The calculated crystallite sizes for the retained austenite and bainite are 85.8 nm and 40.7 nm, respectively, as provided in Table 3.1. The lattice strain of the retained austenite and bainite is estimated as 0.17% and 0.30%, respectively, as mentioned in Table 3.1. The dislocation density is evaluated as $2.64x10^{16}/m^2$ for the retained austenite and $10.39x10^{16}/m^2$ for the bainite phase. The volume fraction analysis of the B14VA-1 sample reveals an estimated composition of

67% retained austenite and 33% bainite, with a calculated volume fraction of 5% for filmy austenite and 62% for blocky austenite, as shown in Table 3.1. Additionally, the carbon concentration in the retained austenite phase is determined to be 1.28 mass%, as indicated in Table 3.1.

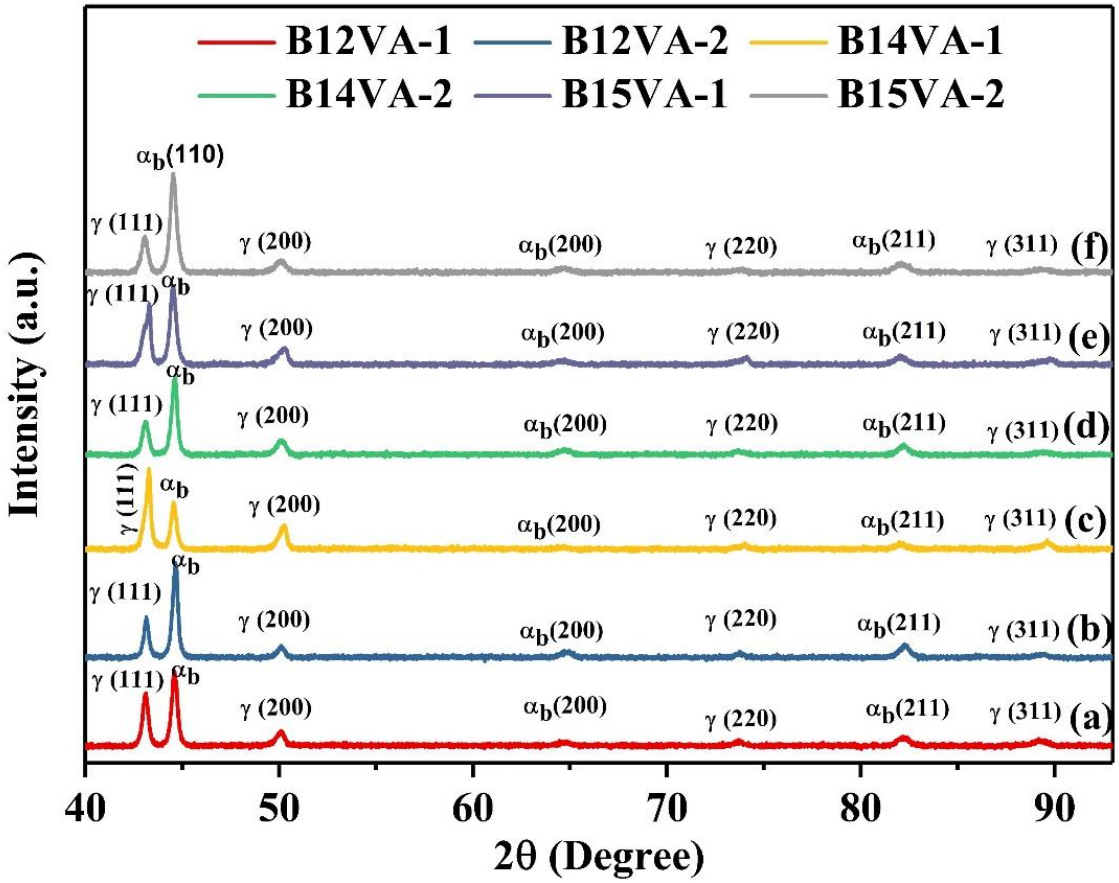

Figure 3.3 X-ray diffraction patterns of the austempered steels : (a) B12VA-1, (b) B12VA-2, (c) B14VA-1, (d) B14VA-2, (e) B15VA-1 and (f) B15VA-2. Here α_b and ϒ stand for bainite and retained austenite, respectively.

Table 3.1 Volume fraction of bainite and retained austenite, crystallite size (C.S.), lattice strain (L.S.), dislocation density (ρ) and C_Y of the austempered steels.

Samples	$V°_{RA}$ (%)	V_B (%)	V_{RA}^F (%)	V_{RA}^B (%)	C.S. (nm)		L.S. (%)		ρ on (111) (x10^{16} /m^2) ϒ	ρ on (110) (x10^{16} /m^2) α_b	C_Y %
					ϒ	α_b	ϒ	α_b			
B12VA-1	48	52	7.8	40.2	46.2	42.1	0.28	0.30	8.28	9.78	1.49
B12VA-2	35	65	9.8	25.3	35.7	36.4	0.35	0.33	13.10	12.66	1.60
B14VA-1	67	33	5.0	62.0	85.8	40.7	0.17	0.30	2.64	10.39	1.28
B14VA-2	35	65	9.8	25.3	30.0	37.8	0.40	0.32	17.92	11.82	1.62
B15VA-1	45	55	8.3	36.8	31.2	33.3	0.39	0.36	16.71	14.89	1.15
B15VA-2	35	65	9.8	25.3	28.3	30.1	0.42	0.39	19.95	17.86	1.73

Figure 3.3d illustrates the XRD pattern of B14VA-2, which displays peaks corresponding to bainite and retained austenite phases. However, the retained austenite peaks in B14VA-2 exhibit lower intensities compared to B14VA-1, and no carbide peak is observed. The estimated crystallite sizes for the retained austenite and bainite are 30.0 nm and 37.8 nm, respectively. The lattice strains of the retained austenite and bainite are determined to be 0.40% and 0.32%, respectively. The dislocation density in the retained austenite and bainite is evaluated as 17.92x10^{16}/m^2 and 11.82x10^{16}/m^2, respectively (Table 3.1). For the B14VA-2 sample, the calculated volume fraction of retained austenite and bainite is 35% and 65%, respectively, with an estimated volume fraction of 9.8% for filmy austenite and 25.3% for blocky austenite (Table 3.1). Furthermore, the carbon concentration in the retained austenite is calculated to be 1.60 mass% (Table 3.1).

Figure 3.3e displays XRD patterns of B15VA-1. The patterns show the peak intensities of bainite and retained austenite. There is no carbide (cementite) peak intensity. The calculated crystallite sizes of retained austenite and bainite are 31.2 nm and 33.3 nm,

respectively (Table 3.1). The lattice strain of retained austenite and bainite are estimated to be 0.39 % and 0.36 %, respectively (Table 3.1). The dislocation density in retained austenite and bainite are evaluated to be $16.7x10^{16}/m^2$ and $14.9x10^{16}/m^2$, respectively. The estimated volume fraction of retained austenite and bainite for the B15VA-1 sample are 45% and 55%, respectively and the calculated volume fraction of filmy austenite and blocky austenite are 8.3% and 36.8%, respectively (Table 3.1). Carbon concentration in retained austenite is estimated to be 1.15 mass % (Table 3.1). Figure 3.3f depicts the XRD pattern of B15VA-2. The patterns of B15VA-2 also show the bainite and retained austenite peaks but lower peak intensities of retained austenite than that of B15VA-1 and no carbide peak. The estimated crystallite sizes of retained austenite and bainite are 28.3 nm and 30.1 nm, respectively. The lattice strains of retained austenite and bainite are 0.42% and 0.39%, respectively. The dislocation density in retained austenite and bainite are $20.0x10^{16}/m^2$ and $17.9x10^{16}/m^2$, respectively (Table 3.1). The calculated volume fraction of retained austenite and bainite for the B15VA-2 sample are 35% and 65%, respectively and the estimated volume fraction of filmy austenite and blocky austenite are 9.8% and 25.3%, respectively (Table 3.1). Carbon concentration in retained austenite is calculated to be 1.73 mass % (Table 3.1).

The XRD pattern of P12VA is depicted in Figure 3.4a and it reveals the peaks of ferrite and cementite only, no extra peaks of other phases are observed. Figure 3.4b shows the XRD spectra of the sample P14VA, and it reveals similar peaks as P12VA sample. The XRD pattern of P15VA, as depicted in Figure 3.4c, exhibits distinct peaks corresponding to ferrite and cementite phases, while no additional peaks indicative of other phases are observed.

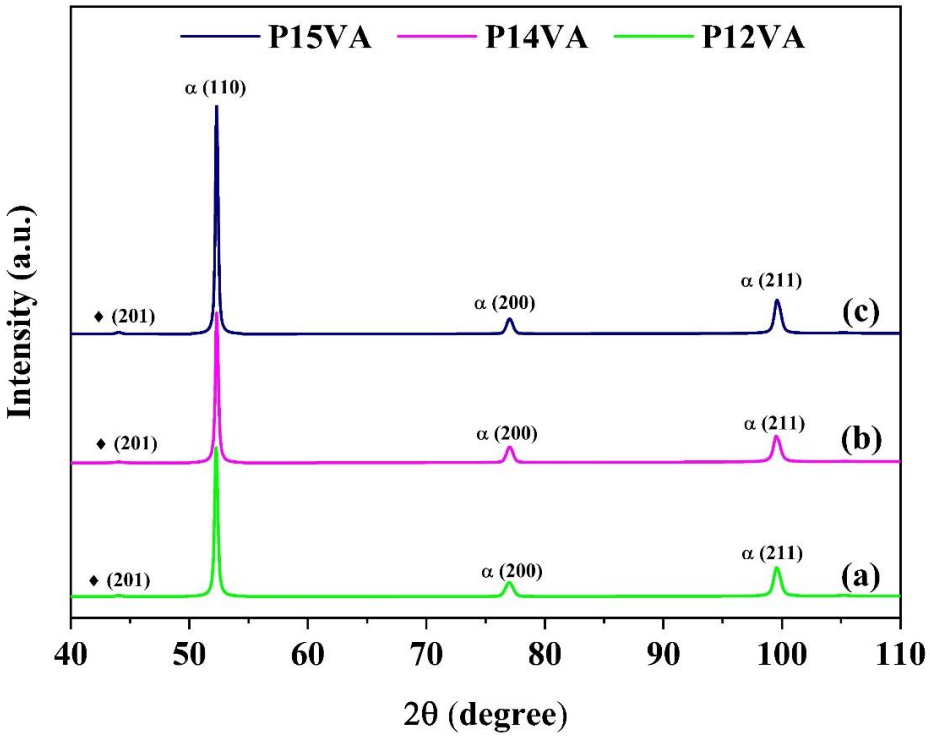

Figure 3.4 X-ray diffraction patterns of the patented steel at 550°C: (a) P12VA, (b) P14VA, and (c) P15VA. Here, α and stand for ferrite and cementite, respectively.

3.3 SEM MICROSTRUCTURE

The SEM images (Figure 3.5a, c, and e) of austempered samples B12VA-1, B14VA-1, and B15VA-1 show a specific microstructure consisting of thin, feather-shaped plates of bainite and filmy retained austenite, with a smaller amount of blocky retained austenite present. The bainite plates and the filmy retained austenite form a sheave-like structure in two-dimensional sections. Between the bainite plates, there is filmy retained austenite, which appears as a thin film-like layer. Additionally, blocky retained austenite can be observed between the sheaves formed by the bainite and filmy retained austenite. The retained austenite refers to the austenite phase that remains untransformed during the heat treatment process.

The polygonal-shaped austenite grains are interconnected and held together by the crystallographic variations present in the bainite sheaves. This microstructural

arrangement gives rise to the observed feathery and blocky morphology in the SEM images. As depicted in Figure 3.5b, d, and f for samples B12VA-2, B14VA-2, and B15VA-2, there is a clear trend of increasing amount of bainite and filmy retained austenite but decreasing amounts of blocky retained austenite with increasing austempering time. The size of the blocky austenite in sample B12VA-1 is 1.26±0.4 μm and it reduces to 1.0±0.4 μm with increasing austempering time to 96 h. The size of blocky austenite in sample B14VA-1 is initially 4.2±1.5 μm, which decreases to 2.0±0.5 μm after an austempering time of 48 hours in B14VA-2. Similarly, in sample B15VA-1, the initial size of blocky austenite is 1.65±0.9 μm, and it is reduced to 0.75±0.3 μm in B15VA-2 after 50 h of austempering.

Figures 3.6a-c depicts the SEM SEIs of pearlitic steel samples P12VA, P14VA and P15VA, respectively and SEIs reveal lamellar pearlitic structure consisting of two phases ferrite and cementite. The material P15VA shows finer microstructure than P12VA and P14VA steels.

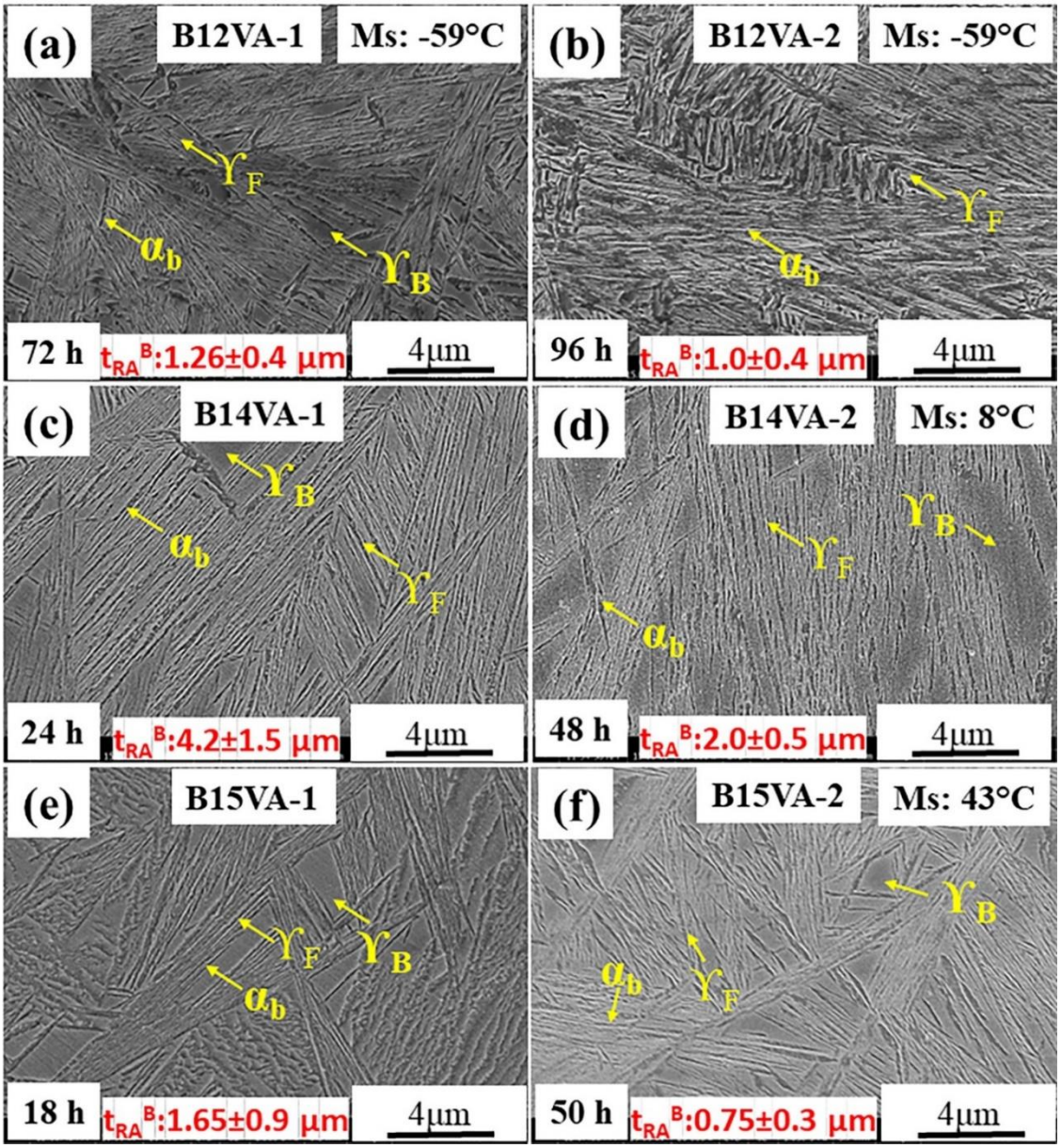

Figure 3.5 SEM secondary electron images (SEIs) of the austempered (at 250°C) bainitic steel (a) B12VA-1, (b) B12VA-2, (c) B14VA-1, (d) B14VA-2, (e) B14VA-1, and (f) B15VA-2. Here α_b, Υ_B, and Υ_F, stand for bainite, blocky retained austenite and filmy retained austenite, respectively.

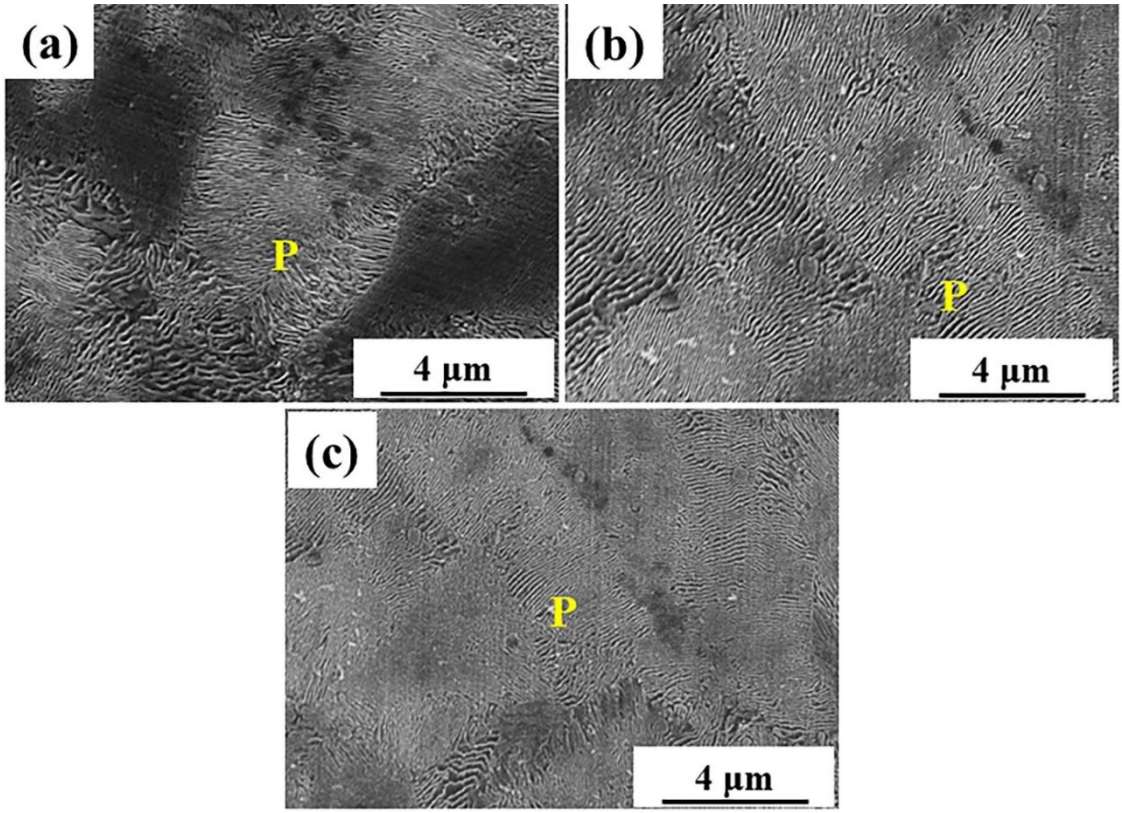

Figure 3.6 SEM secondary electron images (SEIs) of the patented steel at 550°C: (a) P12VA, (b) P14VA, and (c) P15VA. Here P stands for pearlite.

3.4 EBSD ANALYSIS

Electron back scattered diffraction (EBSD) analysis is also utilized to evaluate volume fraction of the existing phases bainite and retained austenite. It is also used to determine qualitatively strain and dislocation density by Kernel Average Misorientation (KAM) map. There is an error of about 10% during the measurement of phase scan during EBSD analysis due to the very finer size microstructure. The volume fraction of the bainite increases with increasing austempering time as depicted in the Figure 3.7a-b, Figure 3.7c-d and Figure 3.7e-f for B12VA, B14VA and B15VA alloys, respectively.

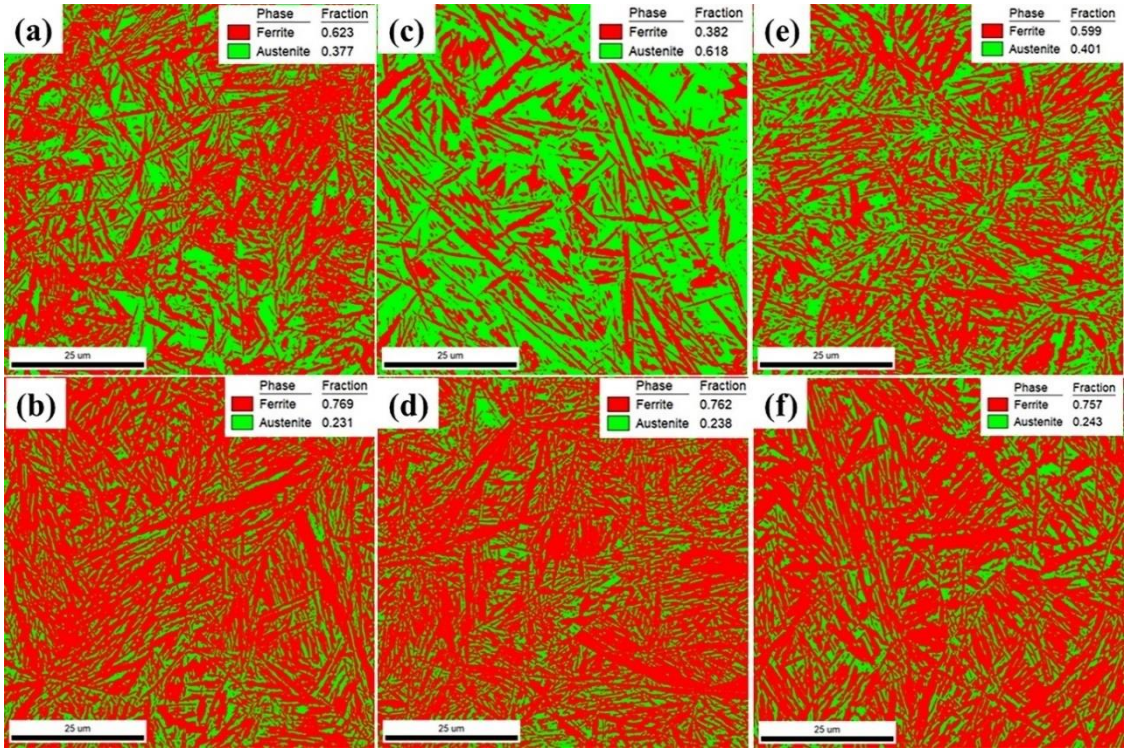

Figure 3.7 EBSD phase map of the austempered steel: (a) B12VA-1, (b) B12VA-2, (c) B14VA-1, (d) B14VA-2, (e) B15VA-1 and (d) B15VA-2.

Figure 3.8 depicts the image quality (IQ) map of austempered samples. IQ map of the sample B12VA-1 is shown in Figure 3.8a, which reveals sheaves of bainite and retained austenite along with ~7% low angle grain boundary (LAGB) and ~68% high angle grain boundary (HAGB). Sample B12VA-2 depicts comparable LAGB and HAGB to that of B12VA-1 sample as presented in Figure 3.8b. Figure 3.8c shows the IQ map of sample B14VA-1, depicting large block of blocky retained austenite and fine bainite along with ~6% LAGB and ~72% HAGB whereas sample B14VA-2 reveals decreased size of blocky retained austenite and bainite with comparable LAGB and increased HAGB to ~75% (Figure 3.8d). IQ maps of samples B15VA-1 and B15VA-2 are depicted in Figure 3.8e and Figure 3.8f, respectively, displays comparable LAGB and increased HAGB from 69% to 72%.

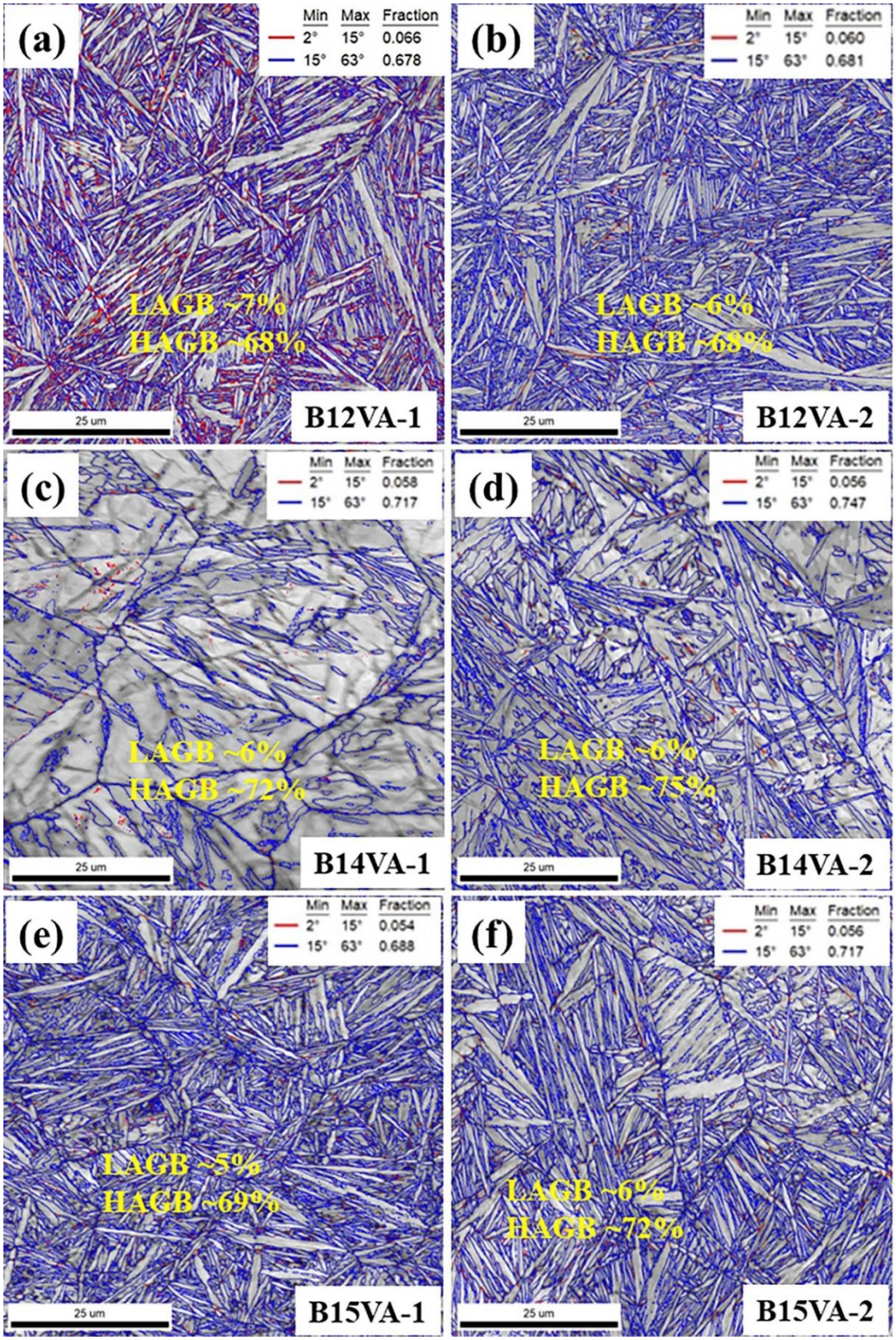

Figure 3.8 Image quality maps of the austempered samples along with LAGB and HAGB: (a) B12VA-1, (b) B12VA-2, (c) B14VA-1, (d) B14VA-2, (e) B15VA-1 and (f) B15VA-2, respectively. Fraction of the LAGB and HAGB are shown in insets.

The inverse pole figure (IPF) map of the austempered sample B12VA-1 and B12VA-2 are presented in Figure 3.9. Figure 3.9a shows the IPF map of the bainite phase which depicts the colour coded sheaves of bainite and blocky retained austenite in black colour region in between sheaves of bainite. Bainite has formed in multiple variants. Figure 3.9b shows the IPF map of austenite phase of the sample B12VA-1, depicting prior austenite grains in colour coded region along with bainite sheaves (black region) inside the prior austenite grains.

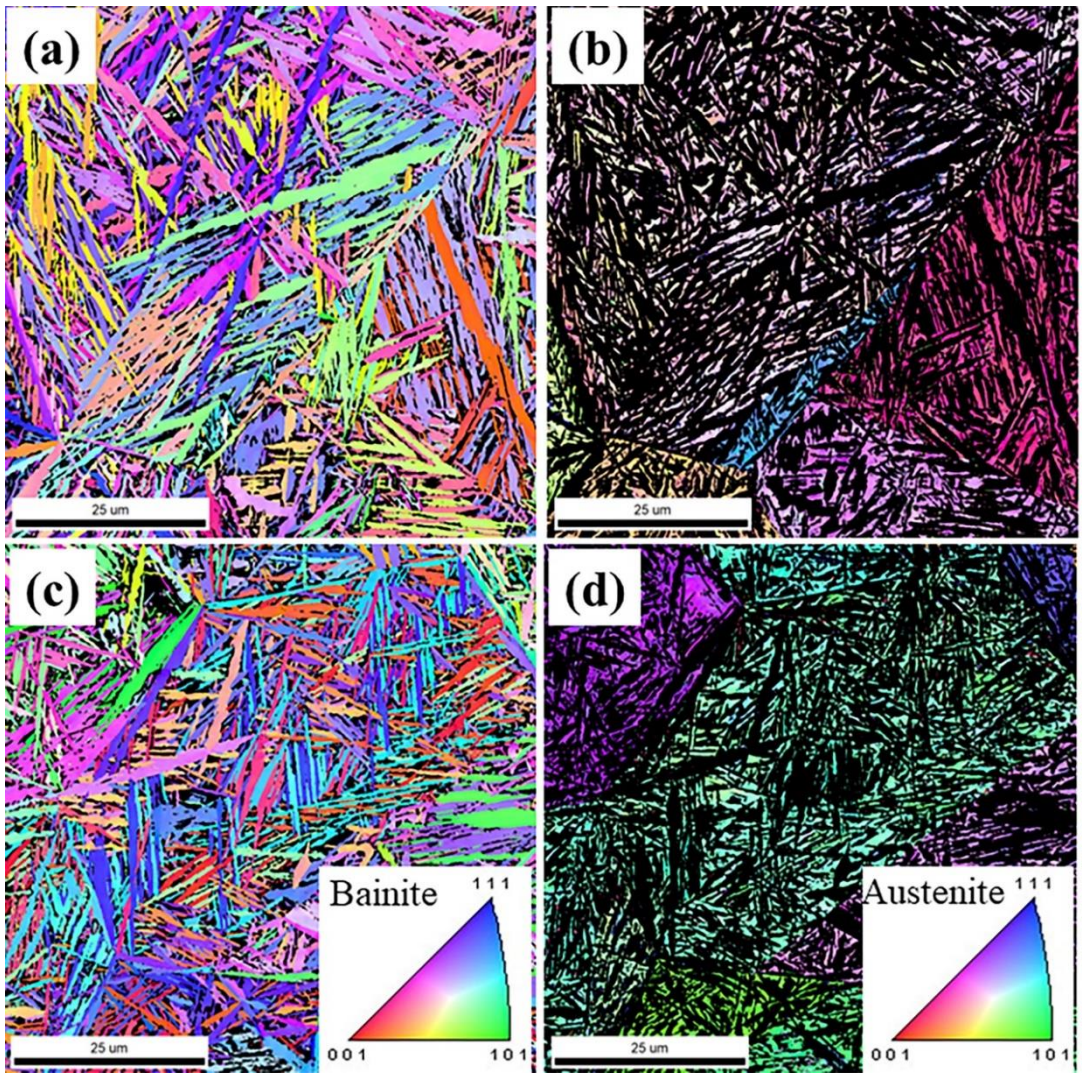

Figure 3.9 Inverse pole figure (IPF) map of normal direction of the sample, B12VA-1: (a) bainite, (b) austenite, B12VA-2: (c) bainite and (d) austenite. Colour codes of IPF maps for bainite and austenite are shown in the insets of Figure 3.8c & d.

Similarly, the IPF map of the bainite and austenite are displayed in Figure 3.9c and Figure 3.9d, respectively depicting similar characteristic to that of sample B12VA-2. The IPF map of bainite phase of B14VA-1 is depicted in Figure 3.9a, revealing large amount of blocky retained austenite (black region) and very small amount of sheaves of bainite (colour coded region) whereas the IPF map of austenite phase shows prior austenite grains (colour coded region) in between some sheaves of bainite are present (black colour region).

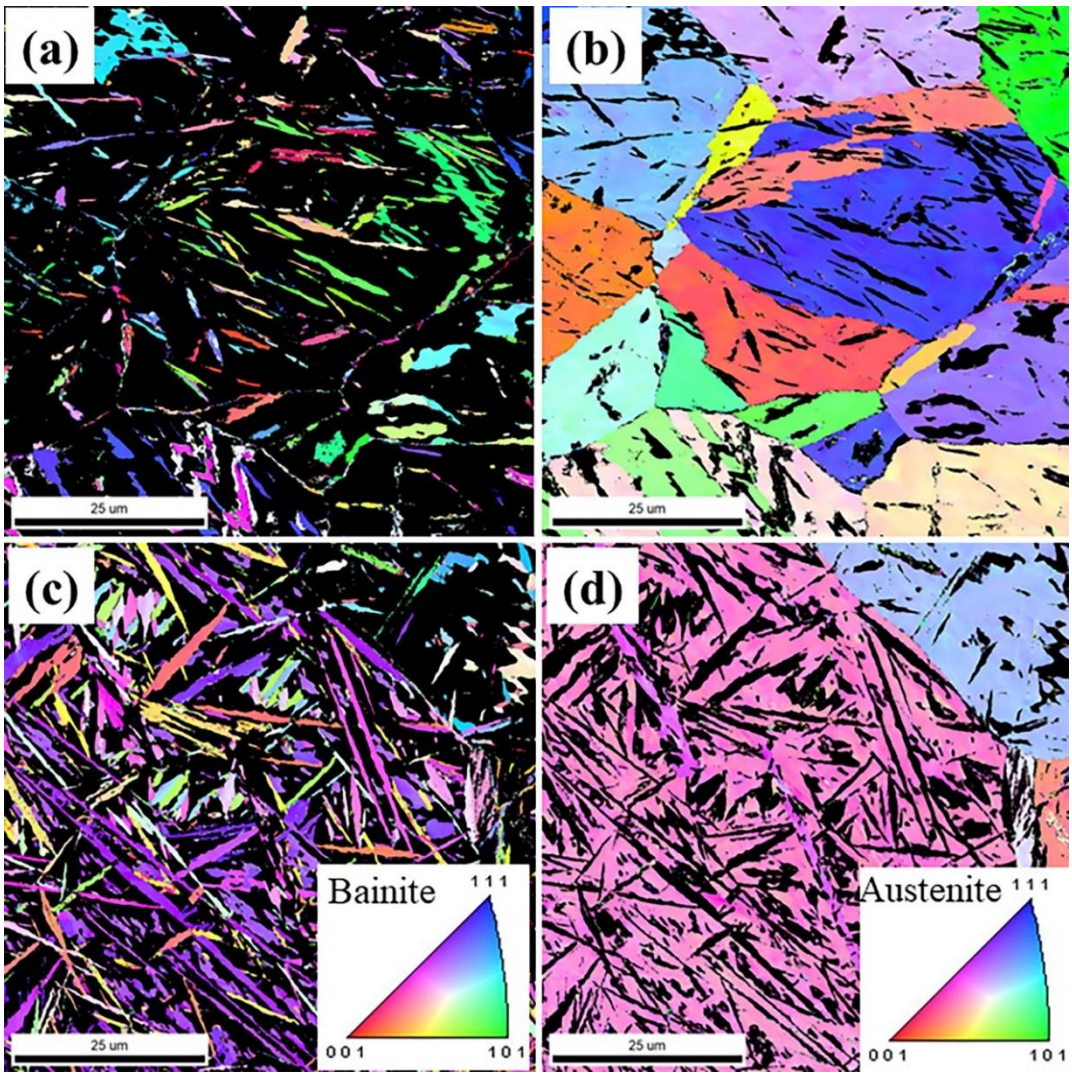

Figure 3.10 Inverse pole figure (IPF) maps of normal direction of the austempered B14VA-1: (a) bainite, (b) IPF of austenite, B14VA-2: (c) bainite and (d) austenite. Colour codes of IPF maps for bainite and austenite are in the inset of Figure 3.10c & d.

Sample B14VA-2 depicts decreased blocky austenite (black region) and increased bainite content (colour coded region) as shown in the IPF map of bainite phase in Figure 3.10c whereas IPF map of austenite phase reveals prior austenite grains and in between bainitic sheaves are present in black region as displayed in Figure 3.10d. Bainite has formed in multiple variants. The IPF map of bainite and austenite phase of sample B15VA-1 and B15VA-2 are depicted in Figure 3.11a-d.

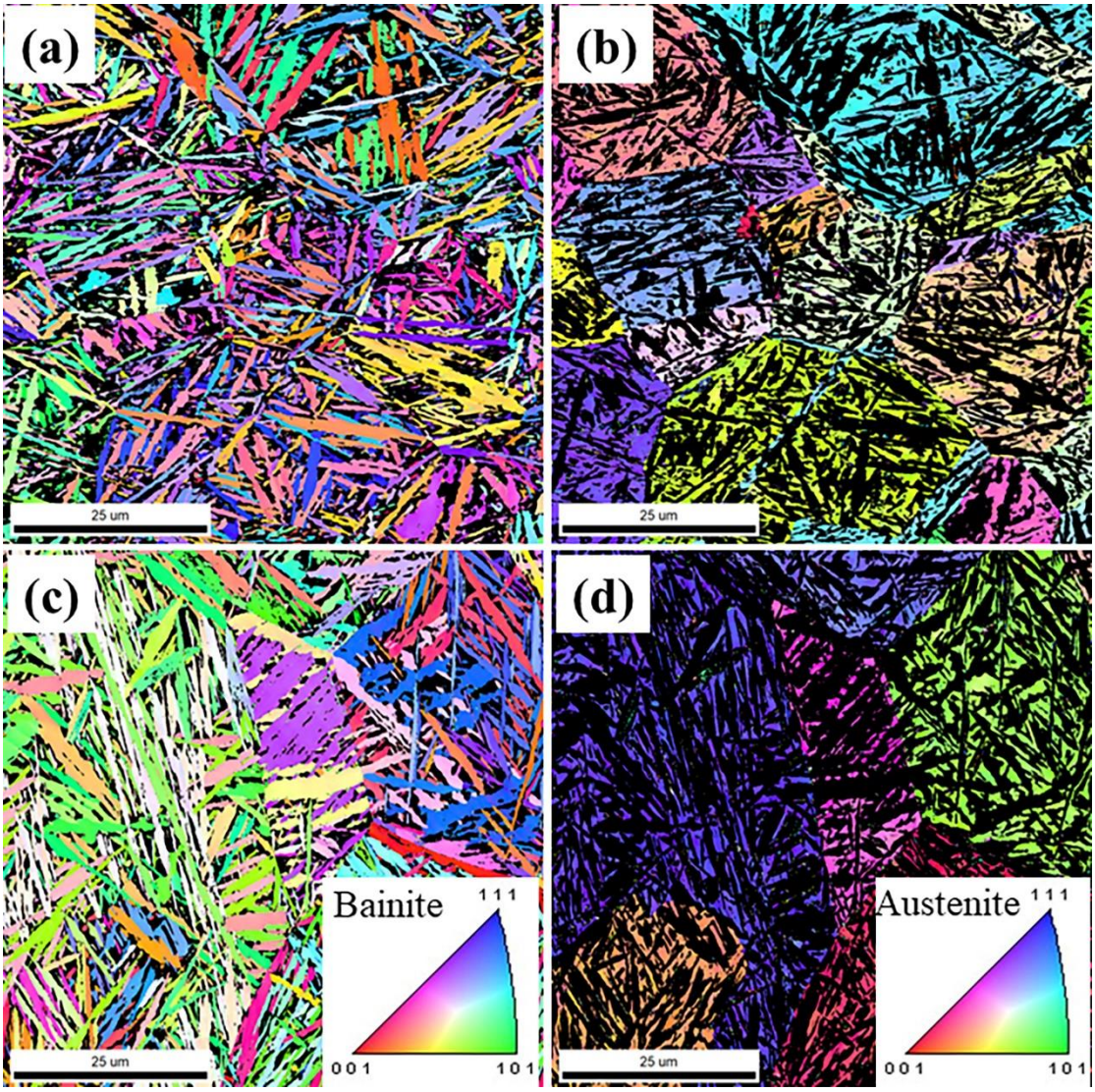

Figure 3.11 Inverse pole figure (IPF) maps of normal direction of the austempered B12VA-1: (a) bainite, (b) austenite, B12VA-2: (c) bainite and (d) austenite. Colour codes of IPF maps for bainite and austenite are shown in the inset of Figure 3.10c & d.

The IPF maps of bainite and austenite phase have similar characteristics to that of B12VA-2 sample.

The KAM map, shown in Figure 3.12, presents qualitative information on strain and dislocation density. A 15x15 μm^2 area is extracted from the original scan data, representing a single prior austenite grain. The strain within this area is calculated based on the 3rd nearest neighbour as the perimeter, with a maximum misorientation angle of 5°. The legend at the top of the figure illustrates the variation of strain across different locations, providing a visual representation of strain levels through a color-coded scale. The KAM map of the bainite phase shows that the strain increases with increasing austempering time from 72 h (B12VA-1) to 96 h (B12VA-2) as shown in Figure 3.12a and Figure 3.12b, respectively.

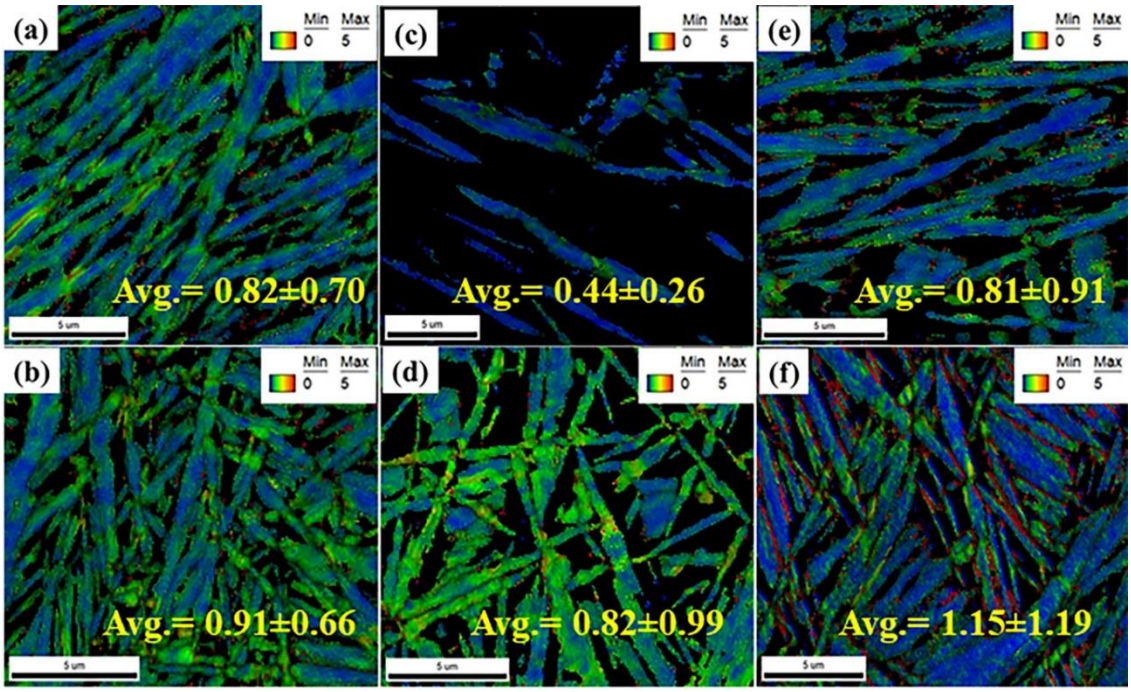

Figure 3.12 KAM maps of the austempered samples: (a) B12VA-1, (b) B12VA-2, (c) B14VA-1, (d) B14VA-2, (e) B15VA-1 and (d) B15VA-2.

Similarly, sample B14VA-1 having lesser bainite content depicting least strain as seen in the KAM map (Figure 3.12c) and strain increases in sample B14VA-2, austempered for higher time i.e., 48 h (Figure 3.12d). Also, the strain in sample B15VA-1 is lesser than B15VA-2 as depicted in Figure 3.12e and Figure 3.12f, respectively.

3.5 TEM MICROSTRUCTURE

The TEM bright-field images (BFIs) of the austempered steel are depicted in Figure 3.13. The BFIs of bainitic steel samples B12VA-1, B12VA-2, B14VA-1, B14VA-2, B15VA-1 and B15VA-2 demonstrate plate-type bainite and both filmy and blocky retained austenite (Figure 3.13a-f) without any carbide. The thickness of bainite plates in the B12VA-1 sample is reported to be approximately 34±9 nm according to Figure 3.13a and Table 3.2. Similarly, B12VA-2 displays bainite plates of thickness 32±9 nm (Figure 3.13b). The filmy austenite in B12VA-1 has a thickness range of 30±8 nm, while in B12VA-2, it is approximately 29±9 nm as indicated in Table 3.2. The thickness of bainite plates in the B14VA-1 sample is reported to be approximately 36±8 nm according to Figure 3.13c and Table 3.2. Similarly, B14VA-2 displays bainite plates of thickness 33±9 nm (Figure 3.13d). The filmy austenite in B14VA-1 has a thickness range of 33±10 nm, while in B14VA-2, it is approximately 32±8 nm as indicated in Table 3.2. The thickness of bainite plates is 24±7 nm for B15VA-1(Figure 3.13e, Table 3.2). The thickness of filmy austenite of the sample B15VA-1 is 22±10 nm. BFI (Figure 3.13f) of B15VA-2 displays the size of bainitic ferrite plates similar to B15VA-1. The thickness of filmy austenite is 21±9 nm (Table 3.2).

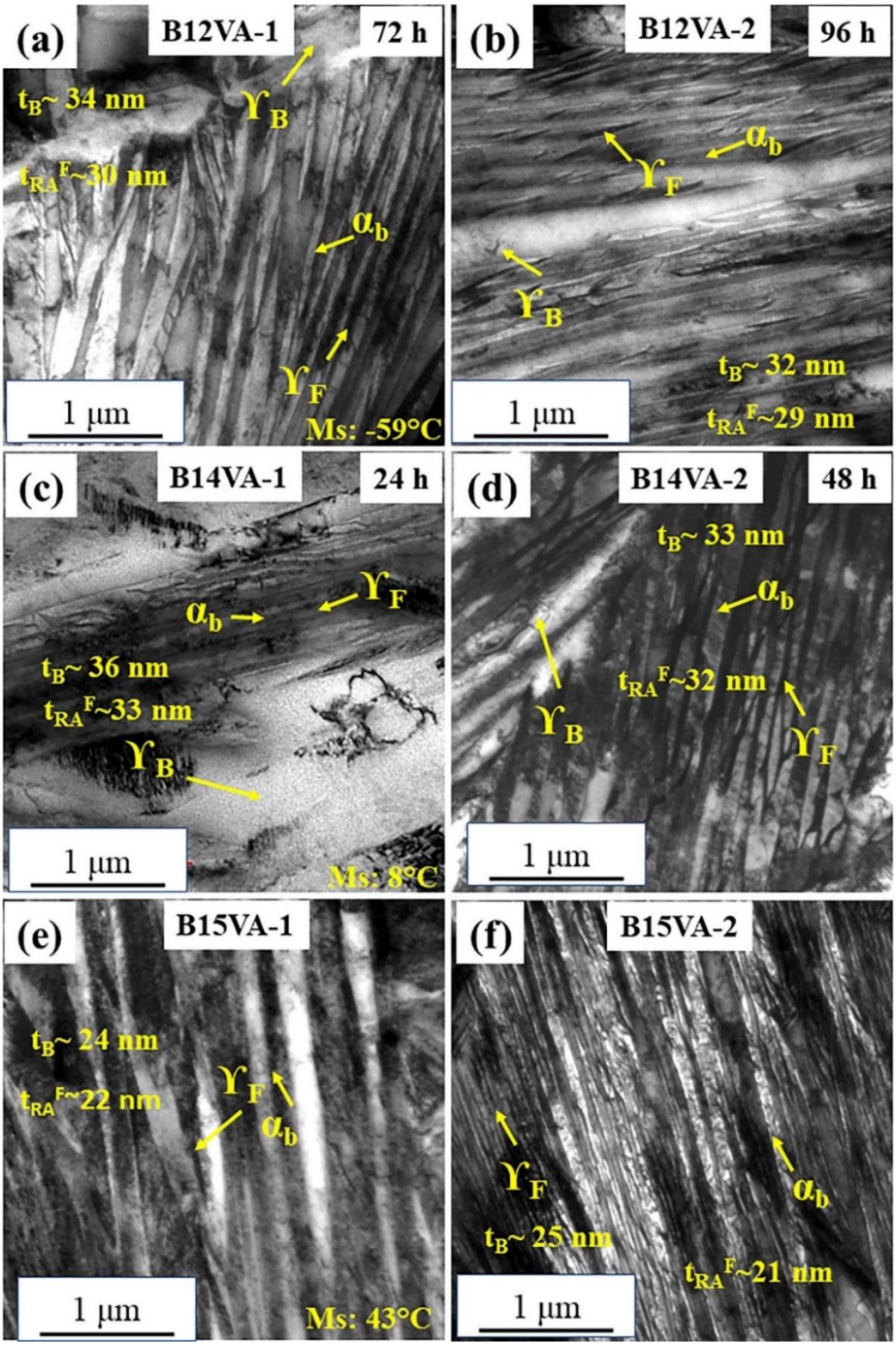

Figure 3.13 TEM bright-field images(BFIs) of the austempered (at 250°C) steels (a) B12VA-1, (b) B12VA-2, (c) B14VA-1, (d) B14VA-2, (e) B15VA-1, and (f) B15VA-2. Here α_b, Υ_B, and Υ_F, signify bainite, blocky retained austenite, and filmy retained austenite, respectively.

Figure 3.14a depicts the BFI of B12VA-2 sample and the inset Figure 3.14a′ displays the magnified view of the selected area of bright-field image (Figure 3.14a) and it does not reveal any carbide precipitate. Selected area diffraction pattern (SADP) of the corresponding BFI (Figure 3.14b), shows spots of bainite and retained austenite but absence of any extra spots for carbides.

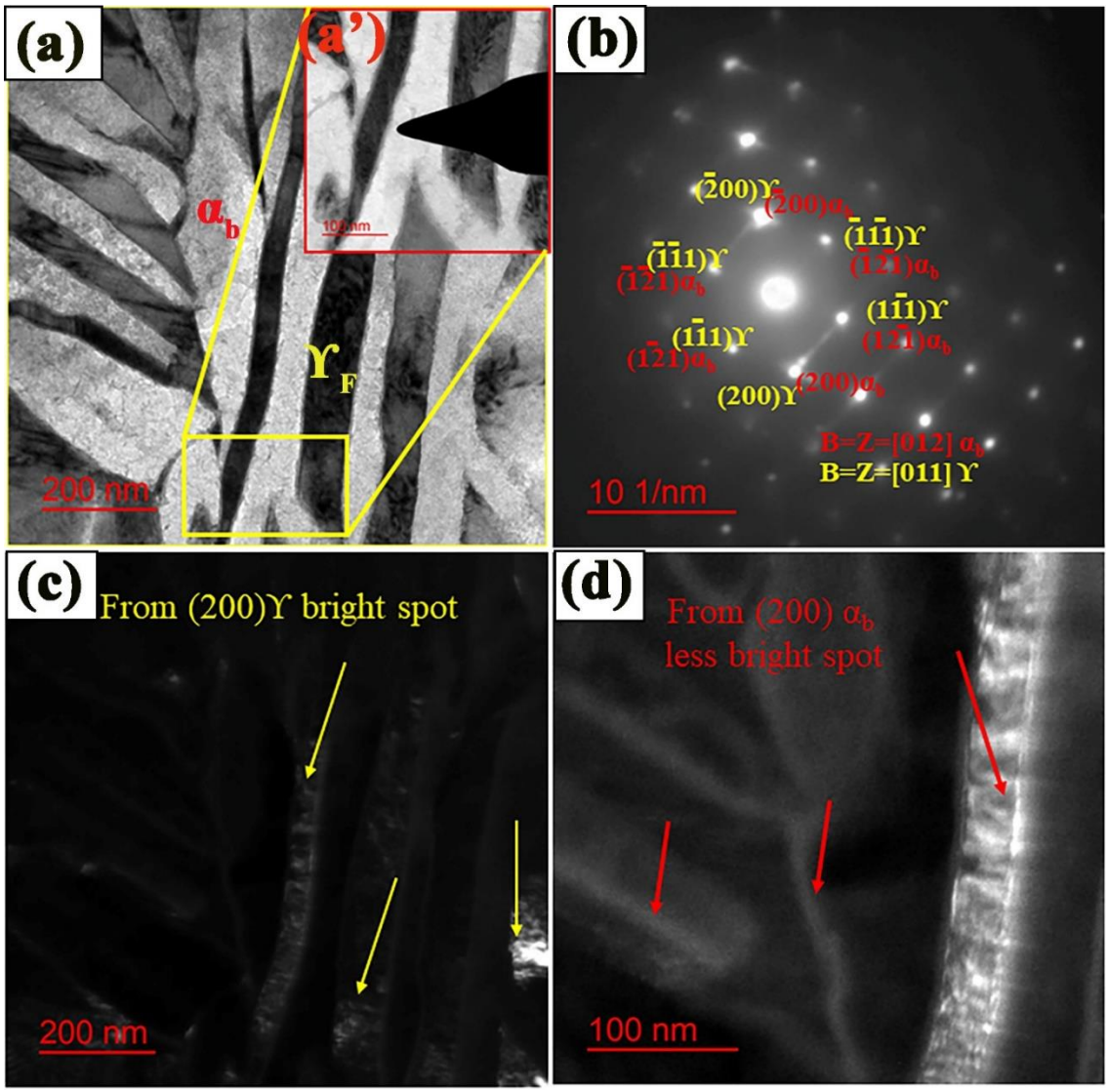

Figure 3.14 TEM micrographs of B12VA-2 (a) BFI, (a′) magnified BFI inset, (b) SADP, (c) DFI from intense spot of (200) Υ, and (d) DFI from less intense spot of (200) α_b.

To separate the contribution in intensity of multiple phases in the selected spot of SADP a dark field image (DFI) is recorded in Figure 3.14c or Figure 3.14d. Figure 3.14c depicts the DFI of intense spot of (200) ϒ and it shows the contrasts for retained austenite only (shown by yellow arrows). Similarly, Figure 3.14d shows the DFI of less intense spot of (200) α_b and it reveals the contrast of bainite plate only (shown by red arrows). Therefore, TEM BFI, SADP and corresponding DFIs confirm the absence of carbides.

Figure 3.15 shows TEM bright-field images(BFIs) and SADP of B15VA-1 and B15VA-2. BFIs display plate-type bainitic ferrite, filmy as well as blocky austenite. Their structures were confirmed by corresponding SADPs. There is no carbide.

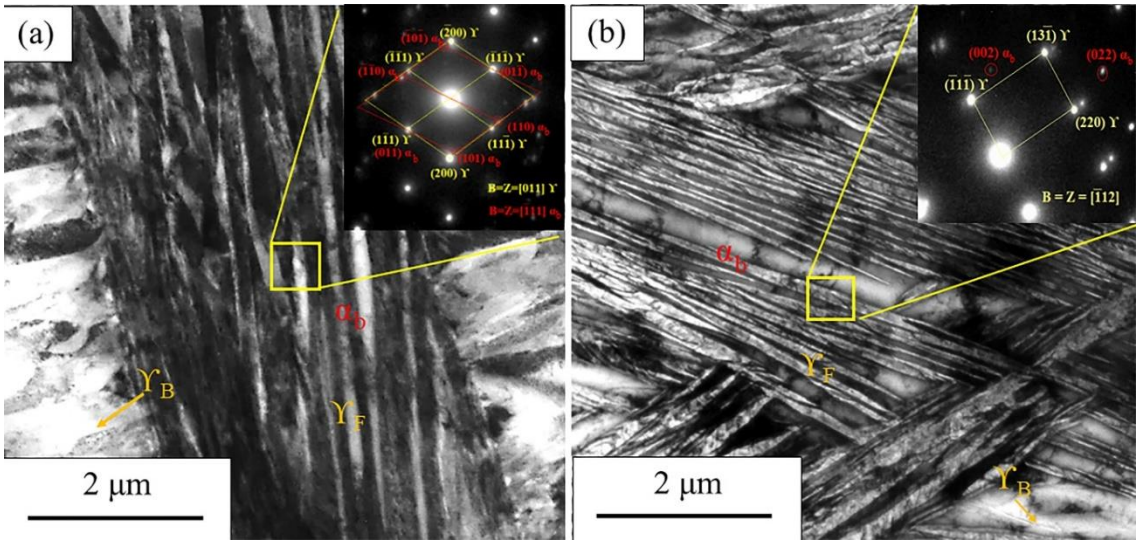

Figure 3.15 TEM bright-field images(BFIs) of (a)B15VA-1 and (b) B15VA-2. SAEDPs are inserted in the corresponding BFI.

Figure 3.16a-c reveals the BFIs of patented steel samples P12VA, P14VA, and P15VA. BFIs of pearlitic steel specimens P12VA, P14VA and B15VA exhibit lamellar morphology composed of an alternating arrangement of ferrite (white in colour) and cementite (black colour). Inter-lamellar spacing (λ) of pearlitic sample P12VA is approximately equal to 66±14 nm and for sample P14VA is 74±15 nm and P15VA having the lowest value of 38±12 nm (Table 2).

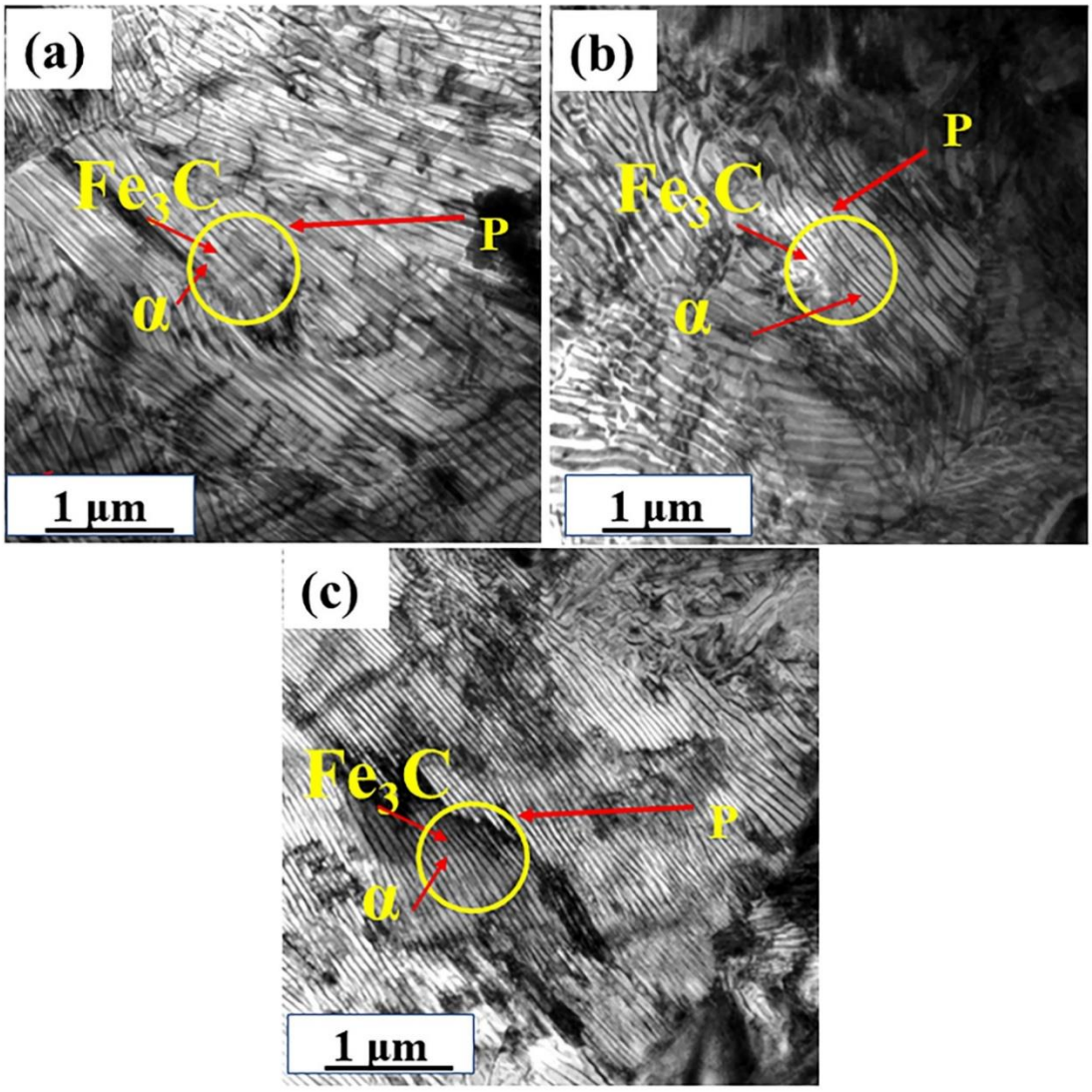

Figure 3.16 TEM bright-field images(BFIs) of pearlitic steel patented at 550°C: (a) P12VA, (b) P14VA, and (c) P15VA. Here P, Fe_3C and α signify pearlite, cementite and ferrite, respectively.

Figure 3.17(a) depicts the TEM BFI of P15VA sample, which reveals the lamellar structure of ferrite (bright colour) and cementite (dark colour). The corresponding SADP of a lamellar region confirmed the presence of ferrite and cementite (Figure 3.17b). Indexed pattern shows presence of ferrite and cementite spots. Yellow net of spots is for ferrite and red one is for cementite.

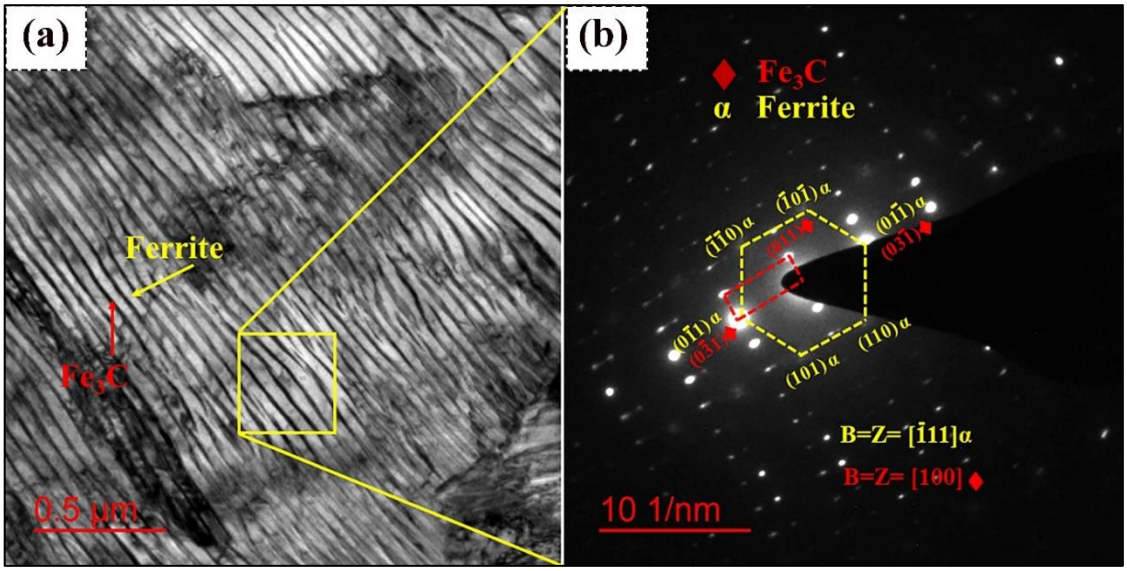

Figure 3.17 TEM micrographs of pearlitic steel (a) BFI of P15VA sample, a selected area in BFI marked by yellow square box is used for SADP and corresponding (b) SADP of P15VA. In this indexed pattern yellow net of spots indicates for pearlitic ferrite and red coloured net is for pearlitic cementite.

Table 3.2 Microstructural features of austempered and patented steels.

Samples	Thickness of bainite plate (t_B), nm	Thickness of filmy retained austenite plate (t_{RA}^F), nm	Size of blocky retained austenite (t_{RA}^B), µm	Inter lamellar spacing (λ), nm
B12VA-1	34±9	30±8	1.26±0.35	-
B12VA-2	32±7	29±9	1.0±0.35	-
P12VA	-	-	-	66±14
B14VA-1	36±8	33±10	4.2±1.50	-
B14VA-2	33±9	32±8	2.0±0.50	-
P14VA	-	-	-	74±15
B15VA-1	24±7	22±10	1.65±0.90	-
B15VA-2	25±9	21±10	0.75±0.26	
P15VA	-	-	-	38±12

3.6 DISCUSSION

Composition is designed in such a way that the required amount of bainitic ferrite can be obtained at the austempering temperature in reasonably less time. Transformation time of selected composition are obtained from JmatPro database for 1-50%

transformation at the selected austempering temperature (250°C). The data are utilized to calculate approximate timing of required transformation amount.

The new alloys were designed based on the composition of Fe-C-Si-Mn-Mo-Cr-Ni-Co-Al to achieve carbide-free nanostructured bainitic steel by austempering at a low possible temperature below Bs but above Ms [38,39]. The presence of C, Si, Mn, Cr and Ni lowers the bainitic ferrite start temperature (Bs). The lowering of Ms temperature by most of the above elements except Co and Al resulted in decreasing of Ms temperature. Austempering of designed steel at low temperature (250^{o}C) produces feathery morphology of nano-scale bainitic ferrite plates of 24-38 nm thick and retained austenite. The hardenability of steel was improved with the addition of alloying elements such as Cr, Mn and Ni to stop reconstructive transformation by air cooling. Mo avoids tempered embrittlement [151]. Low austempering temperature provides a low rate of bainitic ferrite transformation. Al and Co are added to increase the transformation kinetics of bainitic ferrite formation [2].

The study of microstructure and phase analysis confirms formation of carbide-free nanostructured bainite with filmy as well as blocky austenite in the selected steels after austempering at 250°C. It was reported that to prevent carbide precipitation at 250°C in a Fe-1.2C-Si-Mn alloy under para-equilibrium situations, a minimum of 2.0 mass% Si is necessary [34]. The selected alloy has lower carbon % (<1.2%) but Si content is more than 2.2%. The presence of high Si content prevents carbide precipitation at 250°C. These findings are consistent with literature. Low temperature of austempering produces nanostructured bainite. With increasing austempering time the content of bainite increases and size as well as volume fraction of blocky austenite decreases though decreased rate of transformation due to enrichment of carbon in austenite. Bhadeshia and

Singh [152] demonstrated that at the same transformation temperature, the thickness of bainite plates was mostly determined by the preserved austenite strength and chemical-free energy. Carbon-enriched strong retained austenite and a large driving force result in a narrow, lower-temperature bainite plate. In bainitic steel, the thickness of bainite plates ranges between 24 and 38 nm. A lower austempering temperature promotes the formation of retained austenite with a filmy shape inside the subunits of bainitic sheaf. In contrast, blocky austenite is observed in between bainite sheaves [39, 153]. As austempering duration increased, content of blocky austenite is reduced.

On the other hand, high Si is unable to stop cementite precipitation during patenting treatment at 550°C which is much higher than that of austempering temperature. The XRD spectra and microstructure study of the patented samples demonstrated the presence of ferrite and cementite. Patenting of selected hypereutectoid steels P12VA and P14VA at 550°C for 1 hour produces 100% lamellar pearlite of interlamellar spacing 66-74 nm. With addition of austenite stabilizer Ni of 0.43 mass% in P15VA, the interlamellar spacing decreases significantly to 38 nm due to higher stability of austenite [121].

Lattice strain and dislocation density in retained austenite increase with austempering time due to the progress of bainitic ferrite transformation, which contributed in improving hardness and tensile yield strength. Also, the retained austenite peak intensities were decreased and the corresponding bainitic ferrite peak intensities were increased.

3.7 CONCLUSIONS

Based on detailed microstructural analysis using various techniques, the following findings can be derived:

1. X-ray diffraction and transmission electron microscopy studies of austempered steel confirm that the investigated steels are carbide-free.
2. Austempering of specially designed B12VA (Ms: -59°C), B14VA (Ms: 8°C), and B15VA (Ms: 43°C) steels at 250°C results in carbide-free nanostructured bainite with plate thickness in the range of 24-36 nm along with filmy and blocky retained austenite.
3. For a given composition and austempering temperature, increasing austempering time increases volume fraction of bainite, increases amount of filmy austenite but decreases blocky retained austenite.
4. For a B12VA composition and austempering temperature of 250°C increasing austempering time from 72 h to 96 h increases volume fraction of bainite from 48% to 65%, increases amount of filmy austenite from 7.8% to 9.8% but decreases blocky retained austenite from 40.2% to 25.3%.
5. For a B14VA composition and austempering temperature of 250°C increasing austempering time from 24 h to 48 h increases volume fraction of bainite from 33% to 65%, increases amount of filmy austenite from 5% to 9.8% but decreases blocky retained austenite from 62% to 25.3%.
6. For a B15VA composition and austempering temperature of 250°C increasing austempering time from 18 h to 50 h increases volume fraction of bainite from 55% to 65%, increases amount of filmy austenite from 8.3% to 9.8% but decreases blocky retained austenite from 36.8% to 25.3%.

7. Austempering of B12VA, B14VA and B15VA steels for a respective optimized period of 96 h, 48 h and 50 h at 250°C temperature produces ~65 % bainite and 35% retained austenite.
8. The patenting treatment of the investigated steels at 550°C provides 100% fine pearlitic microstructure with inter-lamellar spacing in the range of 38-74 nm.